Attractor vicinity decay for a cellular automaton

James P. Crutchfield and James E. Hanson

Citation: Chaos **3**, 215 (1993); doi: 10.1063/1.165986
View online: http://dx.doi.org/10.1063/1.165986
View Table of Contents: http://scitation.aip.org/content/aip/journal/chaos/3/2?ver=pdfcov
Published by the AIP Publishing

Attractor vicinity decay for a cellular automaton

James P. Crutchfield and James E. Hanson
Center for Complex Systems Research, Beckman Institute for Advanced Science and Technology, University of Illinois, Urbana, Illinois 61801[a)]

(Received 3 September 1992; accepted for publication 4 February 1993)

The temporal decay of an attractor's vicinity for a domain-wall dominated cellular automaton (CA) is studied. Using selected initial pattern ensembles, state space structures in this high-dimensional nonlinear spatial system can be identified via the resulting decay to its attractors. Considered over a range of lattice sizes, the decay behavior falls into three main classes, each of which shows a characteristic profile. The first consists of even-size lattices showing a decelerating decay to small nonattracted ensemble fractions. The second class, also for even lattices, is a catastrophic decay to very small or vanishing nonattracted fractions. The third class also shows catastrophic decay and contains all odd-size lattices. Stochastic models are constructed that mimic the behavior of typical lattices throughout their evolution until finite-size effects appear. Weak additive noise causes all states on all lattices to fall into the attractor. In the end we find it overwhelmingly likely that the recently proposed attractor-basin portrait captures the CA's qualitative dynamics.

I. STATE SPACE GEOMETRY AND RELAXATION PROCESSES

The state space geometry of large spatial systems is impossible to directly analyze since the dimension is far too high. Some method of projecting onto a space of lower dimension is needed. Existing indirect techniques usually expand with respect to some spatially global pattern function basis, such as Fourier or normal modes.[1–3] These methods are appropriate when there is strong spatial coherence. Localized function bases, such as solitons, can be used for expansion even if spatial coherence is lacking, assuming one knows in advance the appropriate functional form for the solitons.[4,5] Roughly speaking, the state space geometry in these cases consists of nested tori whose local coordinates describe the relative phase information of the solitons' motion. An alternative approach for studying high-dimensional state spaces is to design initial condition ensembles that probe subspace structures controlling relaxation dynamics.[6] Notably, this is independent of the presence or absence of spatial coherence. In the following we apply this method to a very simple class of spatial systems, cellular automata (CA).[7] The particular example analyzed exhibits strong spatial decorrelation, but is nonetheless highly structured, with spatial patterns consisting of chaotic domains separated by diffusing walls.

In an attempt to capture the state space geometry of high-dimensional systems, we recently proposed a computation theoretic framework for investigating the qualitative dynamics of extended systems. The attractor-basin portrait of a cellular automaton was given in terms of formal languages that described pattern ensembles.[8] Continuing in this vein we investigate here various decay processes revealed by the relaxation of selected initial pattern ensembles. The focus is on the statistical properties that control the stability of the CA's regular attractors. The primary goal in this and in a companion work is to quantitatively demonstrate that exceptions to the attractor-basin portrait analysis, though inevitably present, represent a vanishingly small fraction of initial conditions and lattice sizes. A secondary motivation is to address several of the simpler issues that will arise in the future development of techniques for identifying state space structures in high-dimensional nonlinear spatial systems.

II. CELLULAR AUTOMATA

Many CA exhibit "domains" of homogeneous spatio–temporal structure that are separated by "walls." In the following we take the nearest-neighbor elementary CA (ECA) rule 18 as an exemplar of this large class. It is arguably the simplest nonlinear CA. The neighborhood patterns {001,100} at time t map to a center cell of value 1 at time $t+1$; all others map to 0. Unlike other chaotic CA such as ECA rule 90, ECA 18 does not obey a linear superposition principle. This is the sense in which it is nonlinear.

The domains of ECA 18 have a simple property: Every other cell is 0. Between those sites are "wild-card" sites that can be either 0 or 1. Its walls break this spatial symmetry with a pattern of $1(00)^n1$, $n=0, 1, 2, \ldots$, which places a 1 on a site that, if it were in a domain, should have a 0. Thus, for example, two consecutive 1s separate two domains: One domain has 0s on even sites; the other, 0s on odd sites. We refer to these walls as dislocations. Figure 1 shows the temporal evolution of ECA 18 dislocations starting from an arbitrary initial pattern using a "filtered" space–time diagram that factors out the intervening chaotic domains.

The dislocations appear to move randomly: At each time step they must move either left or right, the choice being determined (ultimately) by bits in the initial condition. When two dislocations are sufficiently near they can annihilate by merging into a $10(00)^n1$ pattern, a nonlinear

[a)]Permanent address: Department of Physics, University of California, Berkeley, CA 94720; J.P.C.'s Internet address is chaos@gojira.berkeley.edu; J.E.H.'s is hanson@gojira.berkeley.edu.

 1054-1500/93/020215-10$06.00

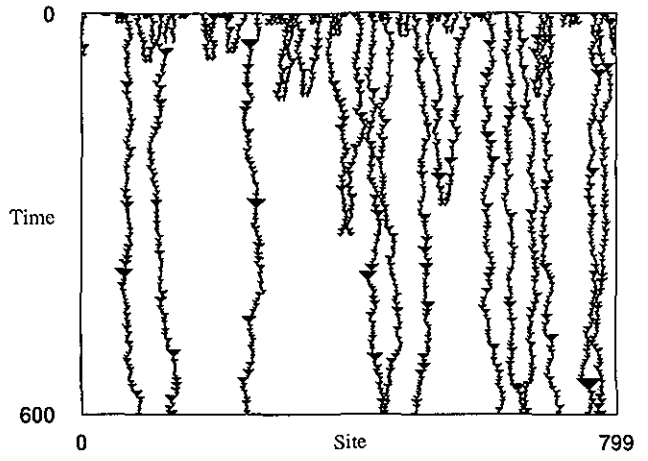

FIG. 1. The temporal evolution of dislocations $1(00)^n1$ under elementary cellular automaton 18, starting from an arbitrary initial pattern. The diagram was produced using spatial transducers from Ref. 8. The chaotic domains have been factored out leaving the dislocations highlighted.

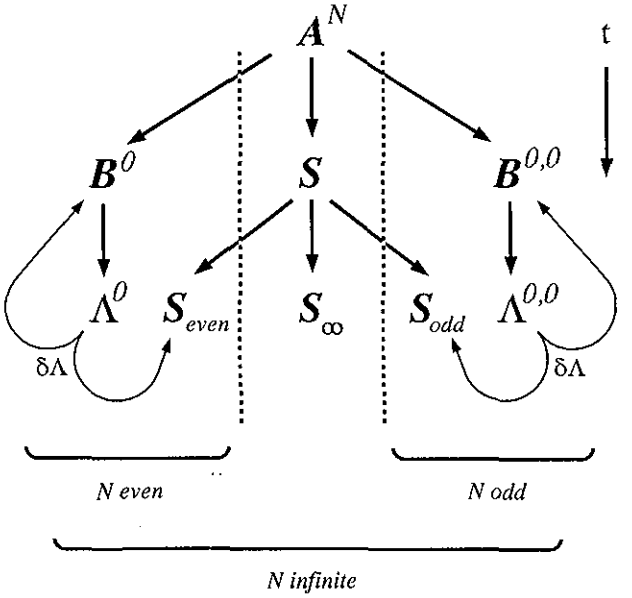

FIG. 2. A skeletal picture of rule 18's attractor-basin portrait. The view is that in language space and includes both finite odd and even lattices along with infinite lattices. The various symbols indicate the formal languages identified in the computation theoretic analysis of Ref. 8. The temporal evolution from one language to another goes down the page. The thin lines with arrows indicate the effect of perturbations $\delta\Lambda$ away from the attractors. Figure reproduced from Ref. 8.

and irreversible process. It gives rise to the apparent nonlocal annihilation seen, for example, near the center of Fig. 1. Starting from an arbitrary initial pattern ECA 18 appears as a gas of randomly diffusing, annihilating dislocations superposed on a chaotic background.[9] The motion of a single dislocation between two semi-infinite (random) domains recently was shown to obey a random walk.[10] Similar results for two or more dislocations are substantially more difficult to obtain since the dislocations' motion eventually becomes correlated due to the overlap of their reverse-time light-cones. This difficulty lies at the root of the problem we investigate here and is one reason the semi-empirical approach we take is a necessary complement at this time to the rigorous analysis.

An algebraic analysis of CA has recently begun to address some of the robust properties due to nonlinearity and strong dislocation interactions. For example, it has been shown that ECA 18 patterns with dislocations can be linearized.[11] The algebraic techniques describe much of the combinatorial structure of the discrete state space of CA on finite lattices. The number and type of periodic orbits for ECA 18 on a given lattice size can be determined, for example.[12] Not surprisingly, the detailed behavior is highly sensitive to the number-theoretic properties of the lattice size N, such as its prime factorization. This leads to large fluctuations in the calculable properties as a function of lattice size that can obscure common features of the CA's behavior.

III. QUALITATIVE DYNAMICS

The qualitative dynamics of a dynamical system is the description of the state space in terms of attractors, basins, and separatrices.[13,14] This gives a picture of the global architecture of state space, without attempting to find closed-form solutions of an individual pattern's evolution. The discreteness of CA state space and the spatial nature of CA pose a number of problems for this type of analysis. Nonetheless, a general procedure for constructing attractor-basin portraits of CA that overcomes many of the problems has recently been developed and applied to the particular case of ECA 18 (Ref. 8) and to a wide range of other CA.[15]

One useful feature of this qualitative analysis is that it traces the development of spatial patterns arising in the CA states, rather than following the exact evolution of any single configuration. This allows for a qualitative characterization of the typical behavior of the system, avoiding the proliferation of details involved in tracking individual trajectories. In addition, it is independent of the particular lattice size and spatial origin. We give a brief synopsis of the results for ECA 18 here.

One view of ECA 18's attractor-basin portrait is shown in Fig. 2. Each symbol in the figure corresponds to an ensemble of CA states with specific properties. On finite, periodic lattices of even size N, only the portion of the figure to the left of the left dashed line is present. For finite odd N, the portion to the right of the right dashed line exists. On infinite lattices, the entire figure is present. At the bottom of the figure are the two attractors, Λ^0 and $\Lambda^{0,0}$. These ensembles are temporally invariant and stable to perturbations. Λ^0 consists of states with no dislocations; $\Lambda^{0,0}$ is made up of states with a single dislocation due to the odd lattice size. The possible effects of small perturbations $\delta\Lambda$ on states in Λ^0 and $\Lambda^{0,0}$ are shown by the thin curving lines. The basins of the attractors, B^0 and $B^{0,0}$, represent the sets of CA states that evolve to some state in Λ^0 and $\Lambda^{0,0}$, respectively. The global separatrix S breaks up into subseparatrices S_{even}, S_{odd}, and S_∞. Finally, A^N, with $A=\{0,1\}$, is the set of all CA states on the lattice.

IV. VICINITY CONVERGENCE

The stability of the attractor under small perturbations is investigated in terms of the attractor's vicinity. Due to the lack of a preferred metric on discrete CA state spaces, there are several alternatives for the vicinity, such as (i) the subbasins b_w with $w=2$ dislocations on even lattices or $w=3$ on odd lattices, or (ii) the Hamming vicinity. The latter, in which perturbations are spatially localized bit-flips, is the more physically realistic of the two if one thinks of the bit-flips as being due to thermal fluctuations. Typical states in the b_w-subbasin vicinity require perturbations correlated over long distances. For this reason, we will focus primarily on the Hamming vicinity in the following. The perturbation we consider, arguably the "smallest" one possible, is a single bit-flip somewhere in the state. If the site flipped is not a wild-card site, this perturbation pushes the state off the attractor by generating a pair of dislocations, which then move about on the lattice and ultimately may or may not collide and annihilate. If and when the dislocations annihilate, the state falls back into the attractor.

Under the action of ECA 18 not all of the patterns in this vicinity fall back into the attractor, even asymptotically. Thus, on lattices with even size N, the vicinity V^0 breaks up into two disjoint subsets, determined by the two possible asymptotic ($t\to\infty$) behaviors: (i) the set E^0 of states that eventually evolve back into the attractor, and (ii) the set P^0 of states that evolve onto temporally periodic orbits not in Λ^0. By definition, $E^0=B^0\cap V^0$ and $P^0=S_{\text{even}}\cap V^0$. In Fig. 2, these two possible asymptotic behaviors are indicated by the two curved lines leading away from Λ^0. For N odd, the situation is analogous, with the vicinity $V^{0,0}$ breaking up into $E^{0,0}$ and $P^{0,0}$. In the following we will consider $\{V,\Lambda,E,P\}$ to be $\{V^0,\Lambda^0,E^0,P^0\}$ for N even, and to be $\{V^{0,0},\Lambda^{0,0},E^{0,0},P^{0,0}\}$ for N odd.

The states in the Hamming vicinity are generated by a two step process. First, a state is produced using the appropriate attractor machine.[8] Second, a site is selected at random and its value is set randomly to 0 or 1. With probability $\frac{1}{2}$ this changes the state; the result may or may not be in the attractor. And with probability $\frac{1}{4}$ a pair of dislocations is created, knocking the pattern off the attractor into the vicinity. The resulting interdislocation distance $d>0$ is distributed exponentially as

$$Pr(d=x)=\begin{cases}2^{-(x+1)/2}, & x=1,3,5,\ldots\\ 0, & \text{otherwise.}\end{cases} \tag{1}$$

An ensemble with M members will have at $t=0$ approximately $M/4$ patterns off the attractor.

A vicinity ensemble's decay can be monitored by the fraction $f_\Lambda(t)$ of ensemble states on the attractor as a function of time. For a fixed lattice size at a given time, we define the complementary fraction $f_P(t)$ of nonattracted patterns in the vicinity ensemble as

$$f_P(t)=\frac{\|\Phi_t(V)-\Lambda\|}{\|V\|}, \tag{2}$$

where $\Phi_t(V)$ is the set of time t iterates of all states in the vicinity V under the CA rule, and $\|L\|$ denotes the cardinality of the set L. The set-theoretic difference $\Phi_t(V)-\Lambda$ denotes the ensemble of states in $\Phi_t(V)$ not yet in the attractor. Clearly, $f_P(t)$ is monotonically nonincreasing with t, and $f_\Lambda(t)+f_P(t)=1$. The asymptotic nonattracted fraction is given by

$$f_P=\lim_{t\to\infty} f_P(t). \tag{3}$$

We define the convergence time T_c as the first time-step at which $f_P(t)$ reaches its asymptotic value. Note that on any given finite lattice $f_P=\|P\|/\|V\|$, the fraction of vicinity states evolving to periodic orbits not in the attractor.

The decay profile $f_P(t)$ gives an indirect indication of the orbit structure of the high-dimensional state space. On a finite lattice with periodic boundary conditions, all states eventually fall onto temporally periodic orbits. In particular, starting from any given initial state $\mathbf{s}_0$ in the vicinity V, the trajectory $\{\mathbf{s}_1,\mathbf{s}_2,\mathbf{s}_3,\ldots\}$ will at some point fall onto a periodic orbit either in the attractor Λ or in the nonattracted set P. If this orbit is in Λ, then there is a time τ at which it first fell into Λ. We therefore define a transient starting in V as a sequence of states $\{\mathbf{s}_0,\mathbf{s}_1,\ldots,\mathbf{s}_{\tau-1}\}$ such that (i) the initial state $\mathbf{s}_0$ lies in the vicinity, (ii) the last state $\mathbf{s}_{\tau-1}$ is not in the attractor, and (iii) the iterate $\mathbf{s}_\tau=\Phi(\mathbf{s}_{\tau-1})$ of the last state is in the attractor. Note that this definition excludes states in P. All states on transients starting in the Hamming vicinity have two dislocations if N is even, or three dislocations if N is odd. The transient length τ is equal to the number of states in that part of the trajectory that lies outside Λ. The fraction of states in the ensemble with transient length τ is given by the instantaneous decay rate

$$\Delta f_P(\tau)\equiv f_P(\tau)-f_P(\tau-1). \tag{4}$$

In this way, the decay curve $f_P(t)$ is the integral of the transient-length probability density. Furthermore, since $f_P(t)$ can change only while there are states on transients, T_c is equal to the length of the longest transient. What $f_P(t)$ fails to capture is the detailed architecture of the state space, i.e., the connectivity of the trajectories.

V. RANDOM CLIFF WALKERS

In ECA 18, the final decay of an arbitrary initial pattern to the attractor usually reduces to the annihilation of only two dislocations. On an even lattice two dislocations collide leaving a pattern in the attractor Λ^0 with none; on an odd lattice two of three collide leaving a pattern in $\Lambda^{0,0}$ with one dislocation. The stochastic analog of the net process is that the dislocations diffuse according to a random walk and two of them eventually annihilate when their paths cross. The question in this view becomes whether ECA 18 with patterns restricted to the vicinity behaves effectively like a stochastic process.

A crude approximation of dislocation evolution, valid in the limit of vanishing dislocation density, was given in Ref. 8. That probabilistic model is inadequate for Hamming vicinity decay since, as just noted in Eq. (1), the dislocation density is weighted toward small separations. As an alternative, we now describe the random cliff walker

TABLE I. Stochastic evolution of the random cliff walker. The distance between particles evolves according to $d(t)=d(t-1)+\delta$.

Random cliff walker	$d(t-1)\leqslant 0$	$d(t-1)>0$
$Pr(\delta=+1)$	0	1/4
$Pr(\delta=0)$	1	1/2
$Pr(\delta=-1)$	0	1/4

(RCW), a simple stochastic process that captures the basic phenomenon. The RCW model, and modifications described below, are variants of a random walk with absorbing barriers.[16,17]

In an ideal random walk a particle moves left or right with equal probability. The distance $d(t)$ between two such particles either stays the same or changes with equal probability. If the distance changes then it is increased or decreased by two units, again with equal probability. In the RCW process two particles annihilate whenever the distance passes through zero. $d(t)$ itself can be considered as a quasiparticle obeying a random walk on the half-line $d>0$. In effect, there is a cliff at the origin: When dislocations annihilate, d passes through zero and the quasiparticle falls off a cliff. This is modeled by stopping the evolution of $d(t)$ at that point, effectively removing one pattern from the ensemble. The rule for the RCW stochastic process is given by

$$d(t)=d(t-1)+\delta, \tag{5}$$

where δ is a random variable with the probability distribution given in Table I. The lattice constant has been changed to $\frac{1}{2}$ so that the possible displacements are $\delta\in\{-1,0,+1\}$. For convenience, we allow $d(t)$ to take on negative values, but require that quasiparticles with $d(t)\leqslant 0$ be frozen in place.

Hamming-vicinity decay is simulated by generating an ensemble of M RCW quasiparticles with an exponential distribution like that for the Hamming vicinity [Eq. (1)], namely,

$$Pr(d(0)=x)=\begin{cases}2^{-x-1}, & x\geqslant 0\\ 0, & x<0.\end{cases} \tag{6}$$

The fraction $f_{\mathrm{RCW}}(t)$ of surviving particles, i.e., those particles i with $d_i(t)>0$, is estimated using the statistic

$$f_{\mathrm{RCW}}(t)=M^{-1}\sum_{i=0}^{M-1}\Theta_i(t),$$

$$\text{where}\quad \Theta_i(t)=\begin{cases}1, & d_i(t)>0\\ 0, & d_i(t)\leqslant 0.\end{cases} \tag{7}$$

A log–log plot of $f_{\mathrm{RCW}}(t)$ vs t is shown as the solid line in Fig. 3. In this and all succeeding plots, the logarithms are base 2. The curve was computed numerically using an ensemble of $M=10\,000$ particles. The curve is of the form $f_{\mathrm{RCW}}(t)=f_{\mathrm{RCW}}(1)\cdot t^{-\alpha(t)}$ with $\alpha(t)\to\frac{1}{2}$ from below as $t\to\infty$. For finite time, $\alpha(t)<\frac{1}{2}$, so that $f_{\mathrm{RCW}}(t)$ shows a slowly downward curving "backbone" whose slope approaches $-\frac{1}{2}$ as $t\to\infty$. A phenomenological model

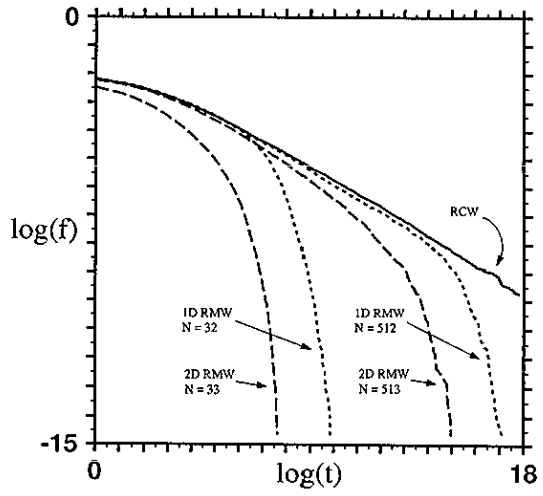

FIG. 3. Decay profiles for annihilating random walks. The random cliff walker decay profile $f_{\mathrm{RCW}}(t)$ is the solid line. 1D and 2D random mesa walker profiles $f_{\mathrm{RMW}}(t)$ are shown for lattices $N\in\{32,512\}$ and $N\in\{33,513\}$, respectively. In this and all succeeding plots, logarithms are base 2. The simulations were performed with ensembles of size $M=10\,000$ for the RCW profile and $M=12\,800$ for each of the RMW profiles.

that gives a reasonable summary of $f_{\mathrm{RCW}}(t)$ uses $\alpha(t)=\frac{1}{2}(1-at^{-b})$ with $a=0.8$, $b=0.15$, and $f_{\mathrm{RCW}}(1)=0.22$.

The $\alpha(t)\to\frac{1}{2}$ convergence can be readily understood. An initial RCW ensemble equivalent to dislocation pairs all starting at the same separation $d(0)=1$ decays like $f_{\mathrm{RCW}}(t)\propto t^{-\alpha}$ with $\alpha\approx\frac{1}{2}$ for all t. The form of $f_{\mathrm{RCW}}(t)$ observed for the exponentially distributed vicinity ensemble is roughly a superposition of the individual decays shifted by the time it takes for the particles to first begin annihilating; the latter is a function of the initial dislocation separation. And so, the decay profile slope gradually decreases until $\alpha=\frac{1}{2}$.

As described, the initial fraction of "active" RCW pairs is $f_{\mathrm{RCW}}(0)=\frac{1}{2}$, whereas the initial fraction of ECA 18 dislocations is $f_P(0)=\frac{1}{4}$. This is due to the fact that an ECA 18 state is perturbed off the attractor with probability $\frac{1}{2}$, and so only half of the states in the vicinity ensemble ever participate in the simulation. This is only a difference in normalization, and is corrected in all of the figures.

In comparing the stochastic model to ECA 18, we will be considering the evolution of dislocations on finite lattices with periodic boundary conditions. For even-size lattices, there are two dislocations, which may annihilate either by approaching each other or by diverging from each other until they wrap around the periodic boundary; for odd lattice size, there are three dislocations, any two of which may annihilate. We treat these two cases as separate modifications of the RCW model. A general model, applicable to any number of dislocations, is a straightforward extension. However, since the vicinities we are studying have only two or three dislocations, the general model is unnecessary and is left for development elsewhere.

For two dislocations, the simpler case, we can include the finite-N effects by adding another "cliff" at lattice site $N/2$ (the factor of $\frac{1}{2}$ comes from the RCW lattice constant,

which is $\frac{1}{2}$). The resulting model is a one-dimensional random mesa walker (1D RMW), which has an explicit dependence on the lattice size. The model's one-dimensional nature is emphasized to differentiate it from the two-dimensional random mesa walker developed below. For an exponential distribution of initial dislocation distances $d(0)$ as above, we expect the fraction of surviving dislocations, $f_{\mathrm{RMW}}(t)$, to show an early epoch during which it follows $f_{\mathrm{RCW}}(t)$, followed by a gradual transition to a second epoch during which $f_{\mathrm{RMW}}(t)$ decays at a faster rate. The transition to the second epoch occurs when the random walkers have had sufficient time to reach the second cliff at site $N/2$. Since the root-mean-square excursion $\sigma = \sqrt{\langle d^2 \rangle}$ of a single random walker evolves as $\sigma \propto \sqrt{t}$, the transition time T_d should vary with lattice size as $T_d \propto N^2$.

1D RMW decay profiles $f_{\mathrm{RMW}}(t)$ vs t for lattices $N \in \{32,512\}$ are plotted on a log–log scale as dotted lines in Fig. 3. For both lattice sizes, the curves were computed numerically using an ensemble of $M = 12\,800$ particles. As the figure shows, $f_{\mathrm{RMW}}(t)$ follows $f_{\mathrm{RCW}}(t)$ up to a deviation time $t \approx T_d$. Numerical experiments on lattices $N \in \{2^k : 3 \leqslant k \leqslant 9\}$ indicated that T_d varies with lattice size as

$$T_d(N) = kN^2, \quad k \approx 0.07. \tag{8}$$

At T_d there is a gradual transition to a faster decay rate. The decay in the second epoch is roughly exponential, with a rate that decreases as N grows larger. In Fig. 3 the transition to the second epoch shows up as a smooth downturn of $f_{\mathrm{RMW}}(t)$ away from $f_{\mathrm{RCW}}(t)$.

The case with three dislocations, corresponding to ECA 18 on an odd-size lattice, requires a more complex modification, since there are three possible ways for the dislocations to annihilate. We can express the evolution in terms of any two of the three interdislocation distances, i.e., $d_1(t)$ and $d_2(t)$. These move according to the stochastic evolution equation

$$d_1(t) = d_1(t-1) + \delta_1, \quad d_2(t) = d_2(t-1) + \delta_2, \tag{9}$$

where δ_1 and δ_2 are random variables with values in $\{-1,0,+1\}$ and with a joint distribution $p(\delta_1,\delta_2)$ given by

$$p(0,0) = 1/4, \quad p(-1,-1) = p(+1,+1) = 0,$$

$$\text{All others: } p(\delta_1,\delta_2) = 1/8. \tag{10}$$

The evolution is subject to the constraints

$$d_i(t) > 0, \quad i = 1,2, \quad d_1(t) + d_2(t) < (N-1)/2. \tag{11}$$

Violation of any of these constraints signifies that a pair of random walkers has annihilated, and so evolution stops at that point. In effect, this is a random walk in two dimensions on a triangular mesa, i.e., a 2D RMW on the simplex defined by Eq. (11). The initial distribution corresponding to Hamming-vicinity decay in ECA 18 has $d_1(0)$ distributed exponentially as for the 1D RMW, and $d_2(0)$ uniform over the interval $1 \leqslant d_2(0) \leqslant (N-1)/2$. Note that a portion of this distribution lies off the simplex, so that some random walkers are already beyond the edge at time zero; this is the same as for ECA 18.

The dashed lines in Fig. 3 show the 2D RMW decay profiles $f^{\mathrm{RMW}}(t)$ vs t for lattices $N \in \{33,513\}$. As for the 1D RMW profiles, the curves were computed numerically using an ensemble of $M = 12\,800$ particles. The curves do not follow the RCW backbone, but rather start some distance below the backbone and curve smoothly downward. The time-1 fraction $f_{\mathrm{RMW}}(1)$ varies with lattice size roughly as

$$f_{\mathrm{RMW}}(1) \approx c_1 - c_2/N \tag{12}$$

with $c_1 = 0.22$ and $c_2 = 1.0$. For each N, the 2D RMW decay profile lies below the corresponding 1D RMW curve, indicating a faster decay rate. As for the 1D RMW case, the decay becomes roughly exponential after an initial epoch. The transition to exponential decay sets in earlier and is much more gradual, making a divergence time more difficult to specify. However, the long-time behavior indicates that the transition has the same lattice-size dependence as does the 1D RMW. This can be observed in Fig. 3 by noting that the exponential tails of the 1D and 2D decay profiles for lattices $N \in \{512,513\}$ are offset by the same amount as for $N \in \{32,33\}$. Data from lattices $N \in \{2^k + 1 : 3 \leqslant k \leqslant 10\}$ indicate that, in the exponential decay epoch, a 2D RMW with lattice size N follows approximately the same curve as a 1D RMW on a lattice of size $N/2$.

If ECA 18 Hamming vicinity decay mimics ideal diffusive annihilation, then its behavior should agree with the 1D RMW stochastic process on even-size lattices, and with the 2D RMW process on odd-size lattices. The temporal decay $f_p(t)$ should follow the same curve as the appropriate $f_{\mathrm{RMW}}(t)$. Conversely, deviations from random mesa walker profiles must be ascribed to other decay mechanisms and state space structures than diffusive annihilation on a finite lattice with periodic boundary conditions. As we show in the next section, Hamming-vicinity decay of ECA 18 typically mimics the stochastic process quite well throughout most of its evolution.

VI. ECA 18 TEMPORAL DECAY

A. Hamming-vicinity decay

Returning now to our investigation of the stability of ECA 18's attractors, we study the temporal relaxation of the Hamming vicinity back onto the attractor in relation to the stochastic decay models. As discussed above, the Hamming vicinity is the physically realistic vicinity to use, since it traces the response of the system to spatially local perturbations.

Hamming-vicinity decay for ECA 18 was investigated for a number of lattice sizes $N < 1000$, largely chosen arbitrarily. For each lattice, an initial vicinity ensemble was created as described in Sec. IV. At each time step each pattern in the ensemble was iterated once. The number of dislocations was counted using the method described in Ref. 8. When the number fell below two, that pattern was removed from the ensemble, since it was in the attractor. States with two or more dislocations were allowed to continue evolving until their dislocations annihilated or they were proven to be on a periodic orbit. The latter condition

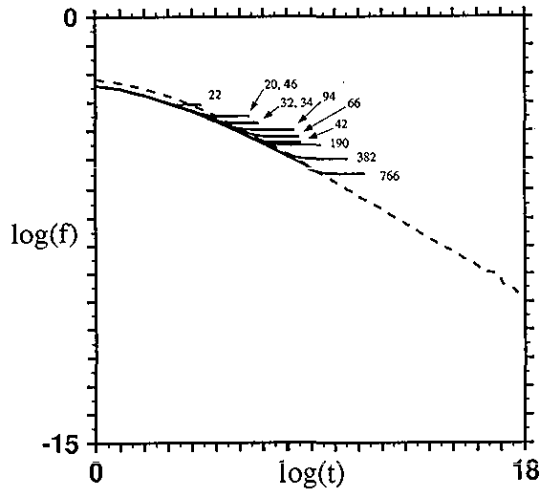

FIG. 4. Decelerating decay (class 1A): $f_P(t)$ for lattice sizes $N \in \{20,22,32,34,42,46,66,94,190,382,766\}$. All curves are labeled by lattice size and plotted to $t=2T_c$. For reference the dashed line gives the rescaled random cliff walker decay $f_{\mathrm{RCW}}(t)$.

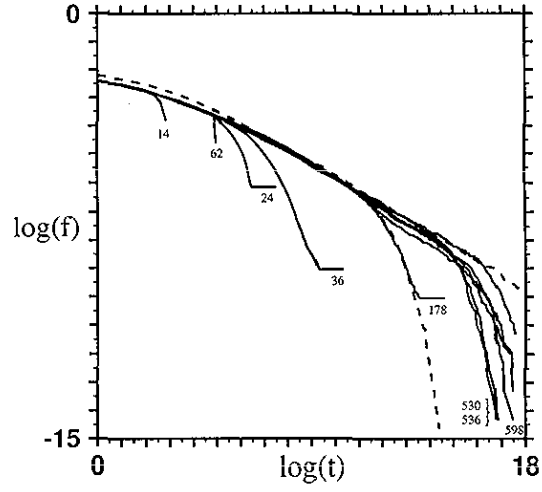

FIG. 5. Catastrophic decay (class 1B): $f_P(t)$ for lattice sizes $N \in \{14,24,36,62,178,530,536,598,790,840,880\}$. Curves for all but the largest three rightmost curves are labeled by lattice size. Lattices $N \in \{24,36,178\}$ have nonzero f_P and are plotted to $t=2T_c$. The three rightmost curves, from top to bottom $N \in \{840,790,880\}$, are plotted to the cutoff time $t=240\,000$. The remaining curves have $f_P=0$ and are plotted to $t=T_c-1$. For reference the upper dashed line gives the random cliff walker decay $f_{\mathrm{RCW}}(t)$. In addition, the random mesa walker decay profile for $N=178$ is shown as the dashed line leading off the bottom of the figure.

was detected using a method described in Ref. 18. At each time, the fraction $f_A(t)$ of states on the attractor was measured, and the nonattracted fraction $f_P(t)$ was calculated according to $f_P(t)=1-f_A(t)$. Vicinity ensemble sizes of $M_1=2\times10^4$, $M_2=1\times10^5$, and $M_3=1\times10^6$ were used. For $N>500$ the ensembles were all of the size M_1; otherwise the size was chosen arbitrarily between M_2 and M_3, and appeared to have little effect on the results, other than reducing statistical fluctuations in the estimated fractions at large times.

We investigated 12 lattice sizes selected to be in the following groups. (1) Worst case.[8,19] The lattices with the largest asymptotic fraction f_P are those with $N_k=3\cdot2^k-2$, $k=0, 1, 2,\ldots$. The difference in size between lattices in this set grows exponentially; we call such sets "sparse." We chose the subset $N_{wc}=\{22,46,94,190,382,766\}$. (2) Winding number $\omega=0$. The winding number ω is the "rotation rate" of spatial patterns on temporally periodic orbits of a finite lattice.[12] Since the nonattracted orbits in the vicinity are all temporally periodic, we initially hypothesized that the winding number might affect the statistics of vicinity convergence. Of the lattices with $\omega=0$ we chose the subset $N \in \{20,24,36\}$. (3) Winding number $\omega=1$: $N \in \{14,31,42\}$. In addition to the above groups, we collected the same statistics on a larger set of 22 arbitrarily selected lattice sizes: even lattices $N_e=\{32,34,66,178,530,536,598,790,840,880\}$ and odd lattices $N_o=\{27,45,77,95,99,213,629,693,781,799,879,919\}$.

Not surprisingly, the decay profiles $f_P(t)$ for even-size lattices showed a characteristic shape different from that of N odd. We label these two classes (I) even-N, and (II) odd-N. In addition, the even-N lattices fell into two distinct subclasses: (IA) decelerating decay and (IB) catastrophic decay. Classes IA, IB, and II are shown, respectively, in Figs. 4, 5, and 6.

All of the even-N lattices follow a common backbone for the early part of their evolution. This backbone closely follows the stochastic RCW decay profile $f_{\mathrm{RCW}}(t)$; the latter is plotted as a dashed line in all three figures. For example, in Fig. 4, the backbone appears as a solid curve lying just below the dashed RCW curve. The time-1 fraction $f_P(1)$ is the same for all lattices in classes IA and IB, but differs from $f_{\mathrm{RCW}}(1)$ by 15%. In addition, the random cliff walker decays slightly more quickly than the ECA 18 backbone, so that the difference between the two grows less

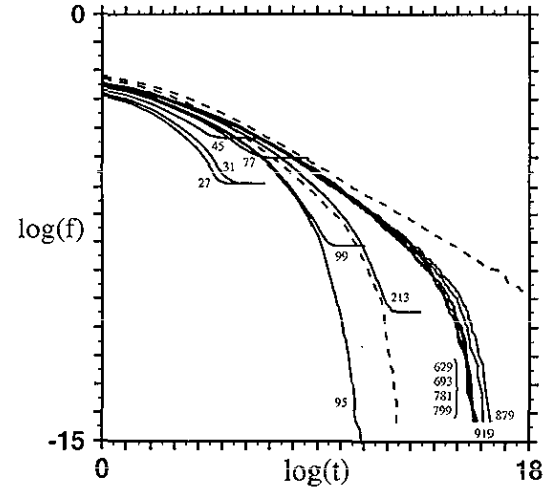

FIG. 6. Odd-N (class II): $f_P(t)$ for lattice sizes $N \in \{27,31,45,77,95,99,213,629,693,781,799,879,919\}$. All curves are labeled by lattice size. Lattices with nonzero f_P are plotted to $t=2T_c$; all others are plotted to $t=T_c-1$. The dashed line lying above all of the decay profiles is the random cliff walker decay $f_{\mathrm{RCW}}(t)$. The 2D RMW curve for $N=213$ is visible as a dashed line curving downward toward the bottom of the plot.

with time. Lattices in class IA remain on the backbone until they approach their asymptotic values. In class IB, each lattice shows a marked downturn away from the backbone before convergence. For nearly all of these catastrophic-decay lattices (with exceptions noted below), this downturn coincides with the RMW's transition to its second (exponential) decay epoch. The convergence of the curves to nonzero values of $f_P(t)$, in Fig. 4 and subsequent figures, is due to periodic orbits in the vicinity that do not fall back into the attractor. The RCW and RMW models do not capture such structure, and so $f_{\mathrm{RCW}}(t)$ and $f_{\mathrm{RMW}}(t)$ continue to decay indefinitely.

The lattices in class IA, the decelerating-decay class, were

$$N\in\{20,22,32,34,42,46,66,94,190,382,766\}. \quad (13)$$

Figure 4 shows a log–log plot of the nonattracted fraction $f_P(t)$ vs t for these lattices. Lattices in this class follow the common backbone of class I lattices for nearly all of their evolution. Near the convergence time T_c there is a gentle leveling as the decay curve makes its final approach to a nonzero asymptotic value. In the figure, the curves have been plotted up to $t=2T_c$ to show the values of f_P. Within the overall class, T_c appears to be roughly proportional to lattice size, and so f_P approaches 0 in the limit of large N. The worst-case lattices N_{wc}, whose asymptotic nonattracted fractions are maximal, fall into the decelerating-decay class.

This class can be characterized as having early convergence, since T_c of each lattice is less than the RMW transition time T_d. The asymptotic fraction is reached before the transition to the second stochastic epoch can occur. For lattices in class IA, the evolution begins to diverge from the stochastic model only during the final approach to the asymptotic limit.

Figure 5 shows $f_P(t)$ for class IB, catastrophic decay. The lattices shown are

$$N\in\{14,24,36,62,178,530,536,598,790,840,880\}. \quad (14)$$

As for class IA, $f_P(t)$ for these lattices initially follows the even-N backbone. At some point there is a transition to a markedly higher decay rate as seen in the profiles' downturn, which continues up to the convergence time. The time at which the transition occurs is within a few percent of the RMW transition time T_d on larger lattices, and within a factor of 2 on the smaller ones. The asymptotic nonattracted fraction f_P can be zero or a finite value. As for class IA, the lattices with nonzero f_P are indicated by horizontal tails extending to $t=2T_c$. The three rightmost curves, $N\in\{790,840,880\}$, were still decaying when the evolution was stopped at $t=240\,000$. The remaining curves have $f_P=0$, and are plotted to $t=T_c-1$.

Two exceptional lattices, $N\in\{14,62\}$, are included in the catastrophic-decay class, even though they converge before the RMW transition time T_d for those lattices. These are the leftmost two downward-pointing curves in Fig. 5. These lattices are members of the sparse set for which all states in the vicinity evolve to the null state 0*. These lattices have size $N=2^k-2$, $k=2,3,\ldots$. Since the null state is in the attractor, $f_P=0$ for these lattices. The sharp downturn in these curves is due to the sudden decay to 0* at time $T_c=(N+2)/2$.

Superimposed on the decay curve for $N=178$ is the random mesa walker decay profile $f_{\mathrm{RMW}}(t)$ for that lattice size. It is shown as the dashed line leading off the bottom of the plot. The agreement between the two curves is remarkable; they overlap nearly all the way to T_c. This is typical of the larger class IB lattices. Smaller lattices tend to diverge from the corresponding RMW curves before T_c. As for class IA, typical lattices in class IB closely agree with the RMW stochastic model for nearly all of their evolution.

The odd-size, class II, lattices

$$N\in\{27,31,45,77,95,99,213,629,693,781,799,879,919\}, \quad (15)$$

plotted in Fig. 6, show the same downward curve as the decelerating decay class, except that they appear to decay more quickly than even lattices of similar size. Some of the lattices have overlapping $f_P(t)$; for example, $N\in\{95,99\}$ lie atop one another until the latter converges to $f_P=0.0035$, and the lattices $N\in\{629,693,781,799\}$ overlap throughout their evolution. Those lattices with nonzero f_P are plotted with horizontal tails to $t=2T_c$, as for classes IA and IB; all others have $f_P=0$.

The time-1 fraction $f_P(1)$ varies with lattice size with roughly the same form as for the 2D RMW, i.e., $f_P(1)\approx c_1-c_2/N$, with $c_1\approx 0.19$, $c_2\approx 1.2$. However, $f_P(1)<f_{\mathrm{RMW}}(1)$ for all lattices; in this, class II is similar to class I. In general, comparison with the 2D RMW decay curves shows that most lattices follow in parallel with the stochastic-model profiles, differing from them by a roughly constant factor. A typical lattice showing this effect is $N=213$, for which $f_{\mathrm{RMW}}(t)$ is plotted in Fig. 6 as a dashed line leading off the bottom of the figure. The ECA 18 decay curve for $N=213$ runs parallel to it until the final approach to the asymptotic fraction. For some lattices, e.g., $N\in\{95,99\}$, the agreement between $f_P(t)$ and $f_{\mathrm{RMW}}(t)$ is nearly perfect.

In summary, then, the Hamming-vicinity decay profiles agree well with the appropriate random mesa walker model, up until they reach the final approach to the asymptotic value f_P. The agreement is increasingly good for larger N. Even-size lattices differ primarily in whether this limit is reached before or after the transition to the second (exponential) epoch of RMW decay. For decelerating decay (class IA), the convergence time T_c is less than the RMW transition time T_d, and the asymptotic fraction f_P is nonzero. For catastrophic decay (class IB) $T_c>T_d$, and f_P is very small or zero. On odd-size lattices, the quantitative agreement with the stochastic model is less good, although the 2D RMW does capture the shapes of the decay curves.

The fact that the decay profiles fall into only a few classes gives some hope to simply describing the geometry of the discrete state space using the qualitative dynamics of Ref. 8 in conjunction with statistical methods. We sketch the beginnings of such a description here; a detailed anal-

ysis will require connecting the discrete state space view with the qualitative dynamics analysis we have used. Recall the discussion at the end of Sec. IV above, which indicated that the convergence time T_c is equal to the length of the longest transient starting in the vicinity, and the instantaneous decay rate $\Delta f_P(t)$ is the same as the probability density of transient lengths. Applying this to the observed decay profiles of the three classes, we see from the convergence times T_c that lattices in class IA have relatively short transients, while for classes IB and II, there exist transients that are much longer: for example, compared to the class IA lattice $N=766$, class IB lattice $N=790$ and class II lattice $N=781$ have transients that are about 500 and 100 times longer, respectively. For all lattices, linear plots of $f_P(t)$ vs t show that $\Delta f_P(t)$ decreases quickly to zero with t. This is especially true of lattices in classes IB and II, for which $\Delta f_P(t)$ decreases exponentially during the second epoch of their evolution. Thus the distribution of transient lengths is sharply peaked at small values; there are many more short transients than long ones. Furthermore, the close agreement between the Hamming-vicinity decay and the random mesa walker profiles shows that for each of classes I and II, the distribution of transient lengths up to the cutoff at T_c is well approximated by a single family of functions parametrized by N.

To get at the large-N, long-time behavior, we observe that the asymptotic fractions f_P are maximal on a sparse set N_{wc} of lattices, and even within this set appear to decrease with lattice size as $f_P \propto N^{-1/2}$.[8,19] Beneath this upper bound, f_P fluctuates wildly with N, indicating sensitivity to the number-theoretic properties of the lattice size. The dependence of f_P on N is exactly the type of question the algebraic analysis should answer; we plan to discuss this in greater detail in the future.

Finally, the decay profiles did not indicate any great dependence on lattice winding number ω, except that $\omega=0$ lattices decay more rapidly than comparable $\omega=1$ lattices.

B. Noisy lattices

As a second method of examining the typical behavior of ECA 18, we added a small amount of random noise to the iteration rule. The extent to which this affects the vicinity convergence profile $f_P(t)$ gives an indication of the stability of the orbits under this perturbation: in particular, of the periodic orbits off the attractor.

The random noise took a particular form, chosen specifically to be the "minimal" perturbation to a state in the vicinity. At each time step, domain wild-card cells are flipped with i.i.d. probability p_{flip}. The latter is set so that approximately one cell in the lattice is flipped per iteration, i.e., $p_{\text{flip}} \approx 2/N$ since there are approximately $N/2$ wild-card cells in a vicinity state. This perturbation does not change the number or the positions of the dislocations. Instead it addresses the questions of whether such a weak perturbation is sufficient to destroy the nonattracted periodic orbits, or whether they are stable, i.e., whether they are themselves attractors.

The overall expectation is that the noise should not affect the decay behavior in the early diffusive epoch. During the later epoch, when the statistics of the noise-free evolution are dominated by the periodic orbits, the stability of those orbits will determine the effect of the noise. If the periodic orbits are unstable, then the asymptotic fraction f_P should decay to zero. Furthermore, the differences in the shape of $f_P(t)$ for different lattices sizes should be less pronounced.

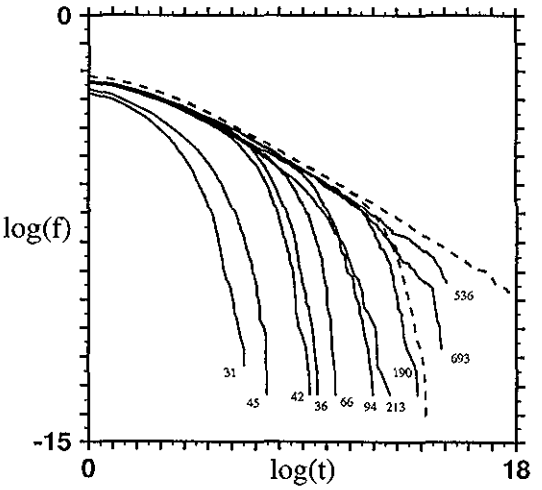

FIG. 7. The effect of noise: $f_P(t)$ vs t for representative lattices $N \in \{31,36,42,45,66,94,190,213,536,693\}$ from each class, with minimal stochastic perturbations in the domains. All curves are labeled by lattice size. Lattices $N \in \{536,693\}$ were halted at $t=30\,000$ before they reached their asymptotic values; all other lattices decayed to $f_P=0$ and are plotted to $t=T_c-1$. As before, $f_{\text{RCW}}(t)$ is shown as a dashed line. The RMW decay curve for lattice $N=190$, which is in the decelerating-decay class for noise-free evolution, is also shown as the dashed line curving down off the bottom of the page.

We gathered statistics for ten lattices $N \in \{31,36,42,45,66,94,190,213,536,693\}$ using ensembles of size $M=1\times10^4$. This group includes examples of all three decay classes defined above. $f_P(t)$ is plotted for these lattices in Fig. 7. Lattices $N \in \{536,693\}$ are plotted to $t=30\,000$; all others are plotted to T_c-1. The results can be summarized as follows.

The two largest lattices, $N \in \{536,693\}$ were still decaying when the evolution was stopped at $t=30\,000$; since both of these lattices have $f_P=0$ for the unperturbed case, we expect the noisy decay to have zero asymptotic value as well. On all other lattices, $f_P(t)$ decayed to zero at finite t. There was no leveling off to a nonzero asymptotic value; the decay profiles for all lattices followed the appropriate RMW curve all the way to $f_P=0$. This difference is most significant in the case of the decelerating-decay (class IA) lattices $N \in \{42,66,94,190\}$, two of which are in the worst-case set N_{wc}. These lattices actually took on the catastrophic profile of class IB. The RMW decay profile $f_{\text{RMW}}(t)$ for the worst-case lattice $N=190$, plotted in Fig. 7 as the dashed line curving down off the edge of the figure, shows a roughly constant offset from the noisy decay profile $f_P(t)$; there is no trace of the decelerating-decay behavior of the noise-free evolution. Neither the catastrophic-decay (class IB) lattices $N \in \{36,536\}$ nor the odd-N (class II) lattices $N \in \{31,45,213,693\}$ were signifi-

cantly affected, up to the time when the unperturbed decay began to level off.

We interpret these results to indicate that the periodic orbits nearby, but not in, the attractors Λ^0 and $\Lambda^{0,0}$ are unstable to small perturbations. The detailed orbit structure imposed by the number-theoretic properties of the lattice size N is washed out by weak noise. Thus, the set of asymptotically nonattracted orbits is sparse in the vicinity: small perturbations typically drive the state into the attractor's basin. This is further evidence that Λ^0 and $\Lambda^{0,0}$ are attractors of ECA 18.

C. Subbasin decay

As we mentioned in Sec. IV, there is more than one possible choice of initial vicinity ensemble. The most obvious alternative to the Hamming vicinity V_H is the b_w subbasin, denoted V_b, which contains all states with $w=2$ dislocations on even-sized lattices and $w=3$ on odd lattices. Clearly, $V_H \subset V_b$. The subbasin vicinity corresponds to the smallest "excitation" of the system, in the sense that the states have the minimal number of dislocations to move them off the attractor. In a parallel series of investigations on the same set of lattices as above, we calculated $f_P(t)$ for an initial ensemble of states drawn uniformly from b_2 or b_3, as appropriate. This induces a distribution of initial interdislocation distances that is uniform, rather than exponentially decaying, as was the case for V_H.

On all of the lattices measured, the convergence time T_c was the same for V_b as for V_H. On lattices where V_H had a vanishing asymptotic fraction f_P, V_b also gave $f_P = 0$. On the remaining lattices, f_P was typically higher for V_b than for V_H. Unlike the Hamming-vicinity profiles, the even-size lattices did not follow a common backbone. Instead, they formed a family of similarly shaped curves parametrized by the time-1 fraction $f_P(1)$. The time-1 fraction increased monotonically with lattice size to a limiting value. The profiles of the lattices fell into the same classification scheme as for V_H decay, but the functional forms were different.

The stochastic model corresponding to the b_2-subbasin vicinity on a lattice of size N is a random mesa walker with a uniform distribution of interdislocation distances $d(0)$ on the interval $0 < d(0) \leqslant N/2$. The probability of a given site being occupied by a random walker is proportional to $1/N$, so that as N grows, relatively fewer random walkers fall off the cliffs in the first time-step. Numerical experiments showed that the time-1 fraction $f_{\mathrm{RMW}}(1)$ varies with lattice size as $f_{\mathrm{RMW}}(1) = c_1(1 - 1/N)$, with $c_1 = 0.25$. The observed decay curves quickly became exponential, $f_{\mathrm{RMW}}(t) \sim 2^{-mt}$, and the decay rate m depended on lattice size as $m(N) = kN^{-\alpha}$, with $k = 16.0$ and $\alpha = 2.0$.

Finally, when a small amount of noise was added to the evolution of V_b, all lattices decayed to $f_P = 0$. All of the decay profiles for even-size lattices were approximately exponential, with a decay rate that decreased with increasing N. As for the RMW model, the decay rate on even-size lattices varied with lattice size roughly as $m(N) = kN^{-\alpha}$, $\alpha \approx 2$, $k \approx 16$; the agreement with the RMW was better for larger N. Odd lattices decayed slightly faster than even lattices of corresponding size.

All of these results indicate that, while the functional forms of the V_b decay profiles differ in details from those of V_H, the convergence times, instability to perturbations, and overall classification scheme are preserved.

VII. CONCLUDING REMARKS

Stepping back then, there are at present three general approaches to analyzing cellular automata: empirical studies using simulation, qualitative dynamics based on computation theory, and algebraic analysis. The preceding work attempted to bridge the gap between these alternative views by relating statistical behavior to the qualitative dynamics, and giving pointers to the relation of those two to the algebraic description. We investigated the diffusive behavior of dislocations as it controls the stability of ECA 18's attractors. The results indicate deviations that should reflect structures accessible via the algebraic analysis. The hope is that, despite the apparent spatio–temporal complexity exhibited by such simple models, much of the structure of nonlinear CA—especially those dominated by domains and walls—can be understood along these lines. At a minimum, though, the empirical results give a quantitative grounding to the actual frequency of occurrence of various phenomena. The earlier discussion[8] of the qualitative dynamics of ECA 18 left several questions unanswered. For example, how likely are deviations from the attractor-basin portrait? And, what fraction of vicinity patterns are not attracted back into the invariant set? The simulations presented here give the quantitative answers to these questions and the random mesa walker, an accurate phenomenological model.

Much of the deterministic CA's behavior is well approximated as an ideal diffusion of a gas of annihilating dislocations. Thus, we interpret the deviations from the stochastic model of temporal decay into the attractor as being indicative of certain state space structures not captured by the attractor-basin portrait; these structures influence the decay on time scales set by the system size and boundary conditions. We found two major types of deviation: (i) final convergence in finite time to a nonzero fraction of states off the attractor; and (ii) systematic deviation by a roughly constant factor throughout the evolution. Both of these effects grow less pronounced as lattice size increases. The decay profiles themselves are closely related to the distribution of lengths of transients starting in the vicinity and falling into the attractor. We found that even-size lattices fall into two classes, one of which has a cutoff at short transient lengths, while for the other, much longer transients are present; odd-size lattices all showed long transients. For all lattices, there were many more short transients than long ones. The interesting observation is that the decay behavior for such a wide range of lattice sizes falls into so few classes. This is a result that is obscured in the discrete state space representation.

The asymptotic nonattracted fraction f_P measures the extent to which states fail to fall into the attractor. Our results show that, as a function of lattice size, the maximal values of f_P decrease as a power law. On very many lattices, especially large ones, f_P decays to 0. Thus in the limit of large N, the size of the nonattracted set goes to zero. A more detailed discussion of the lattice-size dependence of f_P must be left for presentation elsewhere.

In contrast to the deterministic CA, the decay profiles for noisy lattices indicate that the distinctions between the classes are destroyed by very small perturbations to the domains. All vicinity states collapse onto the attractor via a catastrophic decay whose features are captured by the random mesa walker. Thus even minimal noise washes out all deviations from the purely stochastic model. Asymptotically nonattracted orbits, and the state space structures supporting them, appear to exist only for perfectly noise-free evolution; they vanish if even the smallest amount of noise is present. And the latter, presumably, is the physically relevant context for the evolution of ECA 18.

The conclusion is that for moderate to large lattices, the Hamming and subbasin vicinities' nonattracted sets are both insignificant and unstable: Λ^0 and $\Lambda^{0,0}$ are regular attractors.

ACKNOWLEDGMENTS

The authors wish to thank Dan Upper and Karl Young for helpful discussions, and the Beckman Institute and its Center for Complex Systems Research for their generous hospitality. This work was partially funded by ONR Contract No. N00014-92-J-4024 and by a Visiting Research Professorship at the Beckman Institute, University of Illinois, Urbana-Champaign.

[1] P. Manneville, *Dissipative Structures and Weak Turbulence* (Academic, New York, 1990).
[2] B. Shraiman, Phys. Rev. Lett. **57**, 325 (1986).
[3] M. Silber and E. Knobloch, Physica D **30**, 83 (1988).
[4] A. R. Osborne, E. Segre, G. Boffetta, and L. Cavaleri, Phys. Rev. Lett. **67**, 592 (1991).
[5] W. I. Newman, D. K. Campbell, and J. M. Heyman, Chaos **1**, 77 (1991).
[6] J. P. Crutchfield, J. Nucl. Phys. B **5A**, 287 (1988).
[7] S. Wolfram, *Theory and Applications of Cellular Automata* (World Scientific, Singapore, 1986).
[8] J. E. Hanson and J. P. Crutchfield, J. Stat. Phys. **66**, 1415 (1992).
[9] P. Grassberger, Physica D **10**, 52 (1984).
[10] K. Eloranta and E. Nummelin, The kink of cellular automaton rule 18 performs a random walk, Technical Report A296, Helsinki University of Technology, Institute of Mathematics, 1991.
[11] E. Jen, Physica D **44**, 121 (1990).
[12] E. Jen, Nonlinearity **4**, 251 (1990).
[13] D. R. J. Chillingworth, *Differential Topology with a View to Applications* (Pitman, London, 1976).
[14] J. Guckenheimer and P. Holmes, *Nonlinear Oscillations, Dynamical Systems, and Bifurcations of Vector Fields* (Springer-Verlag, New York, 1983).
[15] J. P. Crutchfield and J. E. Hanson, Turbulent pattern bases for cellular automata, Physica D (in press).
[16] F. Spitzer, *Principles of Random Walk* (Van Nostrand, Princeton, 1964).
[17] W. Feller, *An Introduction to Probability Theory and its Applications*, 3rd ed. (Wiley, New York, 1968).
[18] D. E. Knuth, *The Art of Computer Programming: Semi-Numerical Algorithms*, 2nd ed., Vol. 2 (Addison-Wesley, Reading, MA, 1981), Problem 3.1.6.
[19] E. Jen (private communication).